Interval Coding. II. Dendrite-Dependent Mechanisms

Brent Doiron, Anne-Marie M. Oswald and Leonard Maler

J Neurophysiol 97:2744-2757, 2007. doi:10.1152/jn.00988.2006

Journal of Neurophysiology publishes original articles on the function of the nervous system. It is published 12 times a year (monthly) by the American Physiological Society, 9650 Rockville Pike, Bethesda MD 20814-3991. ISSN: 0022-3077, ESSN: 1522-1598. Visit our website at http://www.the-aps.org/.

J Neurophysiol 97: 2744–2757, 2007;
doi:10.1152/jn.00988.2006.

Interval Coding. II. Dendrite-Dependent Mechanisms

Brent Doiron,[1,2] Anne-Marie M. Oswald,[1] and Leonard Maler[3,4]

[1]*Center for Neural Science and* [2]*Courant Institute for Mathematical Science, New York University, New York City, New York; and*
[3]*Department of Cellular and Molecular Medicine, and* [4]*Center for Neural Dynamics, University of Ottawa, Ottawa, Ontario, Canada*

Submitted 15 September 2006; accepted in final form 5 December 2006

Doiron B, Oswald A-M, Maler L. Interval coding. II. Dendrite-dependent mechanisms. *J Neurophysiol* 97: 2744–2757, 2007; doi:10.1152/jn.00988.2006. The rich temporal structure of neural spike trains provides multiple dimensions to code dynamic stimuli. Popular examples are spike trains from sensory cells where bursts and isolated spikes can serve distinct coding roles. In contrast to analyses of neural coding, the cellular mechanics of burst mechanisms are typically elucidated from the neural response to static input. Bridging the mechanics of bursting with coding of dynamic stimuli is an important step in establishing theories of neural coding. Electrosensory lateral line lobe (ELL) pyramidal neurons respond to static inputs with a complex dendrite-dependent burst mechanism. Here we show that in response to dynamic broadband stimuli, these bursts lack some of the electrophysiological characteristics observed in response to static inputs. A simple leaky integrate-and-fire (LIF)-style model with a dendrite-dependent depolarizing afterpotential (DAP) is sufficient to match both the output statistics and coding performance of experimental spike trains. We use this model to investigate a simplification of interval coding where the burst interspike interval (ISI) codes for the scale of a canonical upstroke rather than a multidimensional stimulus feature. Using this stimulus reduction, we compute a quantization of the burst ISIs and the upstroke scale to show that the mutual information rate of the interval code is maximized at a moderate DAP amplitude. The combination of a reduced description of ELL pyramidal cell bursting and a simplification of the interval code increases the generality of ELL burst codes to other sensory modalities.

INTRODUCTION

A central motivation of sensory neuroscience is to identify how specific features of an input stimulus are coded by specific events of a spike train (Perkel and Bullock 1968; Rieke et al. 1997). Many studies have shown that coding schemes of single neurons can be quite complex (Koch and Segev 2000; London and Hausser 2005). This complexity can often be attributed to ensembles of voltage-gated ion channels with specific distributions over the soma and dendrites of a neuron (Reyes 2001; Stuart et al. 1997). Nonlinear dendritic processing influences the gain of spike output in response to static stimuli (Larkam et al. 2004; Mehaffy et al. 2005; Prescott and De Koninck 2003), coincidence detection tasks in auditory brain stem (Agmon-Snir et al. 1998), the capacity for burst response (Larkam et al. 2004; Mainen and Sejnowski 1996; Turner et al. 1994), as well supporting cellular based higher-order computations (Gabianni et al. 2002; Polsky et al. 2004). Theoretical studies have discussed how passive (Tuckwell 1988) or weakly nonlinear dendrites (Maniwani and Koch 1999) shape the neural response to dynamic inputs. However, few studies have addressed how strongly nonlinear dendritic processes, such as those required for action potential backpropagation, influence neural coding schemes for time varying stimuli.

Pyramidal neurons of the electrosensory lateral line lobe (ELL) of weakly electric fish receive direct input from highly reliable receptor afferents (Berman and Maler 1999; Chacron et al. 2005; Wessel et al. 1996). ELL pyramidal cells produce spike trains that consist of isolated spikes and bursts of spikes in response to afferent signals in vivo (Gabbiani et al. 1996; Krahe and Gabbiani 2004; Oswald et al. 2004) and in response to direct somatic current injection of dynamic broadband stimuli in vitro (Oswald et al. 2004). These studies have shown how bursts encode distinct upstroke features of dynamic stimuli compared with those coded by isolated spike events (Gabbiani et al. 1996; Oswald et al. 2004). Expanding on this theme, our companion study has shown how the time interval between the spikes within a burst can code the amplitude and slope of an input upstroke (Oswald et al. 2007).

Complementary in vitro research on ELL pyramidal neurons has identified distributions of voltage-gated sodium channels along the apical dendritic tree (Turner et al. 1994). These channels support active dendritic backpropagation of action potentials resulting in a significant depolarizing afterpotential (DAP) measured at the somatic membrane after a spike; similar phenomena have been observed in a variety of neurons in a number of species (see Reyes 2001; Stuart et al. 1997 for reviews). Furthermore, voltage-gated potassium channels (Fernandez et al. 2005; Noonan et al. 2003; Rashid et al. 2001) and nonspecific leak currents (Mehaffy et al. 2005) over the ELL somato-dendritic axis serve as modulators of the DAP. Several experimental and modeling studies have described a DAP-dependent burst mechanism in response to static stimuli (Doiron et al. 2001–2003; Fernandez et al. 2005; Lemon and Turner 2000; Noonan et al. 2003; Turner et al. 1994). However, only a few studies have discussed the influence of the DAP and the ELL burst mechanism on spike train response to periodic stimuli (Laing and Coombes 2005; Laing and Longtin 2003) or broadband inputs (Oswald et al. 2004, 2007). The extent to which the specific biophysical properties of ELL dendrites contribute to the aforementioned ELL single neuron coding paradigms is not known.

In this study we present a reduced leaky integrate-and-fire (LIF) model of the ELL pyramidal cell that incorporates a DAP mechanism, yet none of the DAP potentiation and dendritic refractoriness that are required for the more biophysically complete ELL-burst mechanisms (Doiron et al. 2001–2003; Fernandez et al. 2005; Noonan et al. 2003). The model repro-

Address for reprint requests and other correspondence: B. Doiron, Center for Neural Science, New York University, 4 Washington Pl., New York, NY 10003 (E-mail: bdoiron@cns.nyu.edu).

The costs of publication of this article were defrayed in part by the payment of page charges. The article must therefore be hereby marked "*advertisement*" in accordance with 18 U.S.C. Section 1734 solely to indicate this fact.

duces the first- and second-order statistics of both the spike train and interspike interval (ISI) sequences observed from in vitro neurons driven with broadband inputs. Furthermore, the model outputs replicate the parallel processing code (Oswald et al. 2004) as well as the interval coding results presented in our companion paper (Oswald et al. 2007). We use this model to study a conceptually simple form of stimulus dimension reduction where the burst ISI codes the effective scale of a basis stimulus upstroke. Using this stimulus representation we compute the mutual information of a quantized ISI-scale code and show the information rate is maximized at a moderate DAP amplitude size. This provides evidence for a further computational role for dendritic excitability during electrosensory processing. The simplicity of both this pyramidal cell model and the ISI-scale code significantly broaden the applicability of ELL-burst codes both within electrosensory processing as well as in comparison with burst coding preformed in other sensory modalities (Krahe and Gabianni 2004).

METHODS

Throughout METHODS and RESULTS we use the notation introduced in our companion study Oswald et al. (2007). Where appropriate we refer the reader to that study for relevant definitions.

Experiments

Recordings from in vitro ELL pyramidal neurons were performed with identical methods detailed in our companion paper (Oswald et al. 2007).

LIF-DAP pyramidal cell model

We represent the ELL pyramidal cell membrane potential with the variable V. The evolution of V is given by the following current balance equation

$$C\frac{dV}{dt} = b - gV + I_{DAC}(t) + \sigma I_{stim}(t) \quad (1)$$

In *Eq. 1*, C and g are the membrane capacitance and leak conductances, respectively, and b is a static current that sets the equilibrium potential in the absence of dynamic inputs. The dynamics of V are supplemented with the standard integrate-and-fire threshold crossing rule (Gerstner and Kistler 2002; Tuckwell 1988): when $V(t) = V_{th}$, then V is immediately reset to V_{reset} and forced to remain there for a refractory period τ_r. After the refractory period, the subthreshold membrane evolution is again dictated by *Eq. 1*. The ith threshold crossing time t is the spike time t_i.

$I_{stim}(t)$ is an applied dynamic stimulus with Gaussian statistics having zero mean and unit SD and broadband spectrum (frequencies distributed with equivalent power between 0 and 60 Hz). σ sets the SD (contrast) of the fluctuating inputs. $I_{stim}(t)$ is identical to that used in the companion study (Oswald et al. 2007) and similar to that used in past investigations of ELL pyramidal cell coding (Bastian et al. 2002; Chacron et al. 2003; Oswald et al. 2004).

ELL pyramidal cells have a punctate distribution of Na^+ channels on their proximal apical dendrite (Turner et al. 1994). These channels support the active backpropagation of somatic spikes along approximately the first 200 μm of the apical dendritic tree (Fig. 1*A*). Rapid somatic spike repolarization ensures that for a brief window of time after a somatic spike the dendrite is more depolarized than the soma. This produces a depolarizing aftercurrent (DAC) that depolarizes the somatic membrane resulting in a DAP; see Fig. 1, *A1–A3*. The function $x(t) = \alpha^2(t - t_i - \tau_{DAC})e^{-\alpha(t-t_i-\tau_{DAC})}\theta(t - t_i - \tau_{DAC})$, low-pass filtered to mimic membrane integration, gives an acceptable fit to the time course of a typical DAP, i.e., $V(t) = A\int e^{-(t-t')/\tau_m}x(t')dt'$ (see Fig. 1*A3*). A is the amplitude of the DAC and τ_{DAC} is a delay that models the time required for a dendritic spike to fire and the return current to source back to the soma. (Lemon and Turner 2000). Here the membrane time constant $\tau_m = C/g$.

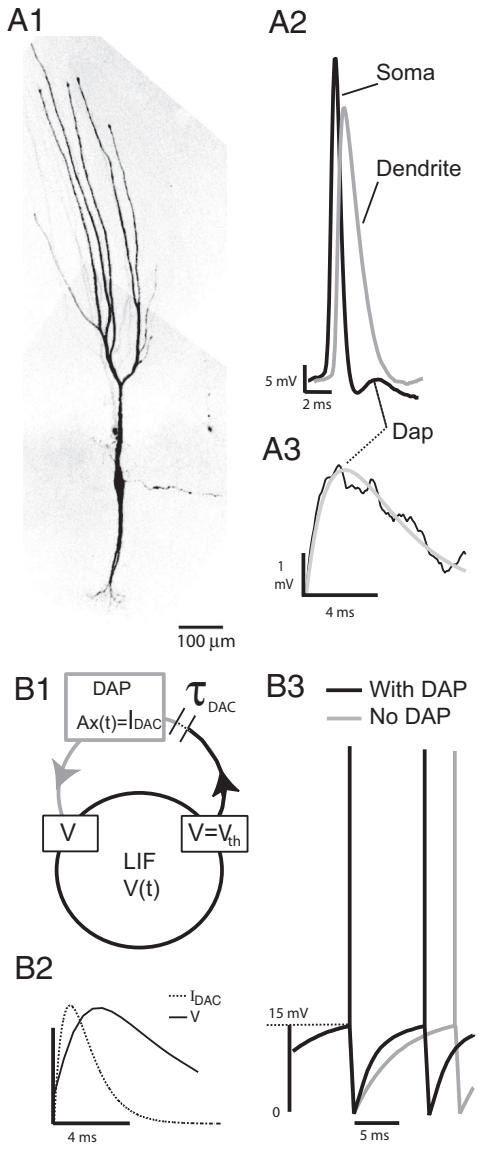

FIG. 1. Leaky integrate-and-fire (LIF)-depolarizing afterpotential (DAP) model. *A1*: confocal image of a Lucifer-yellow-stained basilar pyramidal neuron (Berman et al. 1997). *A2*: somatic and dendritic (~200 μm) action potentials recorded from a pyramidal neuron in vitro (recorded separately). *A3*: potential difference between a control somatic action potential and one with the sodium blocker TTX applied focally to the dendrite. The difference (solid black line) gives the DAP. We fit the DAP with an analytic solution $V(t)$ (gray line), which is a low-pass-filtered depolarizing after-current (DAC) approximation $x(t)$ (dashed line); see METHODS for details. *B1*: schematic of the LIF-DAP model. A threshold crossing of V causes both a membrane reset (standard LIF mechanism) as well as an additional depolarizing input $I_{DAC} = Ax(t)$ after a delay τ_{DAC}. *B2*: model DAC (gray) and resultant model membrane excursion DAP (black). *B3*: model spike trains with $A > 0$ (black) and $A = 0$ (gray). Note that a DAP ($A > 0$) advances the time of the next spike as compared with the model with no DAP mechanism.

We model dendritic activity and DAP production with a strategy that is similar to the one used in Noonan et al. (2003) and Mehaffy et al. (2005). Rather than model the dendritic tree using a cable model (Doiron et al. 2001, 2003) or a reduced two-compartment system

(Doiron et al. 2002; Fernandez et al. 2005), we inject a current waveform I_{DAC} that is representative of the DAC flow occurring after each threshold crossing. We set $I_{DAC}(t) = Ax(t)$ where $x(t)$ given from the fit given in the preceding text. Equivalently, we write the DAC given to the somatic membrane as the auxiliary linear nonautonomous system

$$\frac{dx}{dt} = y \tag{2}$$

$$\frac{dy}{dt} = -\alpha^2 x - 2\alpha y + \alpha^2 \sum_i \delta(t - t_i)\theta(t - t_i - \tau_{DAC}) \tag{3}$$

Given a spike occurs at time t_i, the solution of *Eqs. 2* and *3* with the condition that $x(t_i) = 0$ and $y(t_i) = \alpha^2$ is the fit $x(t)$ stated in the preceding text (shown in Fig. 1*B2*). The coefficient A in *Eq. 1* is the amplitude of the DAC. This process is shown schematically in Fig. 1*B1*. The waveform $x(t)$ and the resultant membrane excursion $V(t)$ with $I_{stim}(t) = 0$ match the membrane potential fit that was obtained from the data (Fig. 1*B2*). This class of model replaces the need to model an independent excitable dendritic compartment and merely models the *effect* of dendritic backpropagation on the somatic membrane via $x(t)$. We compare the membrane dynamics with and without DAP dynamics during spiking activity (Fig. 1*B3*). As expected, the DAP brings the model cell potential closer to threshold (black trace), as compared with the case without a DAP (gray trace), and thus decreases the ISI.

The model parameters were $V_{th} = 15$ mV, $V_{reset} = 0$ mV, $C = 150$ nF, $g = 30$ nS, $b = 0.387$ nA, $\sigma = 0.18$ nA, $\tau_r = 2$ ms, $\tau_{DAC} = 2$ ms, and $\alpha = 0.24$ ms^{-1} (see Mehaffy et al. 2005) (see also RESULTS for parameter justification). Unless otherwise stated, the DAC amplitude $A = 0.855$ nA and the stimulus SD $\sigma = 0.18$ nA. We simulate *Eqs. 1–3* with a fourth-order Runge-Kutta integration algorithm implemented with the simulation package in MATLAB (Mathworks). The random input current I_{stim} was generated off-line with a fourth-order butterworth digital filter using the signal processing toolbox in MATLAB. For model spike train statistics and measures of stimulus coding, we typically computed 30,000–40,000 bursts (10 realizations each of 1,000 s in duration were performed for each data set).

Spike train statistics

From a membrane time series, we construct a point process spike train $s(t) = \sum_i \delta(t - t_i)$ digitized at 2 kHz, where t_i is the time of the ith spike. To measure spike train patterning, we use the zero-mean corrected spike trains $s_m(t) = s(t) - \langle s(t) \rangle$ (where $\langle \cdot \rangle$ is an average over time). The expectation (compared with chance) of observing a spike τ time units after another spike is given by the normalized autocorrelation function $Q(\tau) = \langle s_m(t + \tau)s_m(t) \rangle / \langle \text{ISI} \rangle$ where $\langle \text{ISI} \rangle$ is the mean ISI (Gabbiani and Koch 1998). To quantify the linear transfer properties of spike or burst trains, we use the spectral coherence $C(f) = |S_{sI}|^2/(S_{ss}S_{II})$ (Gabbiani and Koch 1998; Oswald et al. 2004). S_{sI} is the cross-spectrum between the input I_{stim} and the spike train s_m; S_{ss} and S_{II} are the auto spectrums of the s_m and I_{stim}, respectively. $C(f)$ measures the normalized frequency dependent linear input-output correlation between s_m and I_{stim}.

Pattern classification

Pattern classification analysis (Duda et al. 2001) and detection theory (Poor 1994) have been applied to a variety of neural spiking data (Brenner et al. 2000; Gabbiani et al. 1996; Kepecs and Lisman 2003; Metzner et al. 1998; Oswald et al. 2004, 2007). In this section, we introduce a stimulus-reduction ansatz appropriate for the interval coding performed by bursting ELL pyramidal neurons.

In principle, a response with many potential states $R_1, \ldots R_K$ can classify many associated stimulus patterns $\mathbf{s}_1, \ldots, \mathbf{s}_K$. In our companion paper (Oswald et al. 2007), we defined a response set with a quantized burst ISI distribution: a given ISI of length Δ is classified as a response in class R_i if $\mu_{i,i-1} \leq \Delta < \mu_{i+1,i}$, where μ_{ij} is the threshold that separates response state R_i and R_j. Following Oswald et al. (2007), we typically considered only four response groups $R_1, \ldots, R_4$ with $\mu_{01} = 3$ ms, $\mu_{12} = 5$ ms, $\mu_{23} = 7$ ms, $\mu_{34} = 9$ ms. We define a stimulus pattern as the mean of the conditional stimulus distribution $P(\mathbf{s}|R_i)$, where $\mathbf{s}$ is the event-triggered stimulus, i.e., $\mathbf{s}_i = \int \mathbf{s}P(\mathbf{s}|R_i)ds$ (we use a bold notation to indicate a vector). In practice, $\mathbf{s}$ is the K-dimensional vector $\mathbf{s} = [s(t_1), s(t_1 + \Delta t), \ldots, s(t_1 + K\Delta t) = s(t_2)]$ where $K = L/\Delta t$, with $L = t_2 - t_1$ being the time interval of the reverse correlation and Δt the time discretization. It is difficult to compute $P(\mathbf{s}|R_i)$ if the dimensionality of $\mathbf{s}$ is large ($K \gg 1$) as is the case with spike- or burst-triggered stimulus reverse correlations. Our companion paper (Oswald et al. 2007), as well as past studies of electrosensory coding (Gabbiani et al. 1996; Metzner et al. 1998; Oswald et al. 2004), have used feature extraction techniques to reduce stimulus dimension. In brief, the vector members $\mathbf{s}$ of the conditioned distributions $P(\mathbf{s}|R_i)$ and $P(\mathbf{s}|R_j)$ are projected onto a specific feature vector f_{ij}, to obtain the projection length $f_{ij}^T \cdot \mathbf{s}$ is a low-dimensional stimulus representation permitting a reliable estimate of $P(f_{ij}^T \cdot s|R_i)$ and $P(f_{ij}^T \cdot s|R_j)$to be computed from a reasonable sized data set.

In Oswald et al. (2007), $\mathbf{f}_{ij}$ was chosen such that it maximized the discriminability between conditioned events (assuming Gaussian response statistics) (see Metzner et al. 1998). Although this definition of $\mathbf{f}_{ij}$ provided a sensible algorithm for a classifier, interpreting the stimulus after projection onto the feature vector $\mathbf{f}_{ij}$ can be problematic. Specifically, $\mathbf{f}_{ij}$ was a function of both the event-triggered average and covariance (Metzner et al. 1998). Unfortunately, the spike-triggered covariance is a matrix the eigenspectrum of which typically admitted many principle components (typically >10 components were required to capture 95% of the variance). $\mathbf{f}_{ij}$ inherited this complexity, and thus despite feature extraction providing a certain optimality (in the sense of linear discrimination), an intuitive relationship between what the specific differences in the stimulus that event i selects but event j does not select is lacking. To this end, a visual inspection of the $\mathbf{s}_i$ vectors is typically required.

This difficulty of interpretation motivated us to propose a simple stimulus reduction approximation appropriate for the interval code. Consider the burst-triggered average computed from all burst events, $\mathbf{s}_{all} = \int \mathbf{s}P(\mathbf{s})d\mathbf{s}$, where each $\mathbf{s}$ is defined between the first spike of the burst doublet occurring at $t = t_1$ and the second spike occurring at $t = t_1 + \Delta_s$ with Δ_s being the ISI length. Our stimulus reduction is to approximate the stimulus vector during a given burst interval as

$$s \approx \kappa_s s_{all}[1, \ldots, \text{Int}(\Delta_s/\Delta t)] \tag{4}$$

κ_s is a scalar chosen to be the scaling factor is the best fit in the least squares sense, i.e., minimizing $\|\mathbf{s} - \kappa_s \mathbf{s}_{all}[1, \ldots, I(\Delta_s/\Delta t)]\|$ where $\|.\|$ is the Euclidian distance. *Equation 4* effectively assumes that the stimulus that triggers each burst event is just a scaled version of a basis upstroke $\mathbf{s}_{all}$. Int$(\Delta_s/\Delta t)$ is the real number $\Delta_s/\Delta t$ rounded up to the nearest integer. We restrict our comparison between $\mathbf{s}$ and $\mathbf{s}_{all}$ to the components of $\mathbf{s}_{all}$ that occur between the first and second spikes of the doublet. In essence, we assume that the shape of the burst-triggered stimulus is invariant with respect to the stimulus intensity, and it is merely scaled (κ_s) in amplitude. Data presented in our companion paper (see Oswald et al. 2007; Fig. 2*B*) suggest that this is a reasonable approximation. The scalar representation of the reverse correlation by κ_s should be compared with the projection $f_{ij}^T \cdot s$ computed with feature extraction. In RESULTS (Fig. 5), we give empirical evidence for the validity of the approximation in *Eq. 4* for bursting ELL pyramidal neuron spike trains.

To assess coding performance it is typical to employ a simple linear classifier (Duda et al. 2001)

$$h_\theta = g(\mathbf{s}) - \theta$$

where θ is a decision threshold. Here $g(\mathbf{s})$ is either $f_{ij}^T \cdot s$ if the full-feature extraction method is used (Oswald et al. 2007) or it is simply κ_s if the scale reduction is used. If $h_\theta > 0$, then the predicted response is an event in R_j; if $h_\theta < 0$, then the predicted response is an event in R_i. Given M responses, there are $M(M-1)$ feature vectors and one dimensional classifiers; however, because the time separation between events in R_i and $R_{i\pm2}$ is large, then it is sufficient to consider only adjacent stimulus-responses pairs, thereby giving only $M-1$ feature vectors/classifiers. A prediction choice between R_i and $R_{i\pm1}$ requires a specific θ, which in turn defines the probability of correct detection (P_D) and false alarm (P_{FA}) simply as $P_{ij,D} = \int_\theta^\infty P[g(s)]\mathrm{d}[g(s)]$ and $P_{ij,FA} = 1 - P_{ijD}$. The threshold θ that minimizes the error probability $\varepsilon_{ij} = (P_{ij,FA})/2 + (1 - P_{ij,D})/2$ gives the optimal linear classifier. Thus for both techniques the original high-dimensional classification problem has now become a threshold problem dependent on the representation in the relevant stimulus space. Hereafter we suppress the s subscript on κ_s.

ISI code

The assumption of a basis upstroke allowed an intuitive scalar representation of the time-vectored stimuli. In our companion paper (Oswald et al. 2007), we used a quantized description of burst ISI by defining a finite set of burst groups (R_1:3–5 ms; R_2:5–7 ms; R_3:7–9 ms; R_4:9–11+ ms). Given this discrete partitioning of the burst output and our scale description of the burst-triggered stimulus we motivate an appropriately defined quantization of our stimuli (S_1:$\kappa > \kappa_{12}$; S_2:$\kappa_{23} < \kappa < \kappa_{12}$; S_3:$\kappa_{34} < \kappa < \kappa_{23}$; S_4:$\kappa < \kappa_{34}$), where κ_{12}, κ_{23}, and κ_{34} are scale thresholds. We choose these thresholds by minimizing the error probability ε_{ij} for a detection task of a linear classifier (see Fig. 6). Given our discrete one-dimensional response R_1-R_4 and stimulus S_1-S_4, we now can easily compute the joint-probability density $P(S_i,R_j)$, the marginal response $P(R_j) = \sum_i P(S_i,R_j)$, the scale distributions $P(S_i) = \sum_j P(S_i,R_j)$, and the conditional response distribution $P(R_j|S_i) = P(S_i,R_j)/P(S_i)$. The Shannon mutual information (Cover and Thomas 1991) is given as the reduction of response entropy given the stimulus

$$I(S,R) = H(R) - H(R|S) \tag{5}$$

Here the response entropy $H(R)$ and the noise entropy $H(R|S)$ are given by

$$H(R) = -\sum_i P(R_i)\log_2[P(R_i)] \tag{6}$$

$$H(R|S) = -\sum_i \sum_j P(R_i|S_j)\log_2 P(R_i|S_j) \tag{7}$$

Finally, the frequency of burst events (of all groups) is f_{burst}, and we thus compute the information rate as $I_{rate}(S,R) = I(S,R)f_{burst}$.

We remark that an expected source of information loss in our putative interval code is the reduction of $\mathbf{s}$ to κ and the subsequent quantization of κ and the response ISI to the discrete groups S_1–S_4 and R_1–R_4 (Dimitrov and Miller 2001; Dimitrov et al. 2003). More to the point, we fully expect that $I(S,R) < I(\mathbf{s},\mathrm{ISI})$ where $I(\mathbf{s},\mathrm{ISI})$ is the mutual information of the original vector stimulus $\mathbf{s}$ to ISI code. In fact, because the LIF-DAP model is deterministic, then the conditional entropy $H(\mathrm{ISI}|\mathbf{s}) = 0$, which gives the simple result that $I(\mathbf{s},\mathrm{ISI}) = H(\mathrm{ISI})$. However, an appropriate stimulus-response reduction is required to motivate a conceptually simple neural code, such as $S_i \rightarrow R_i$, whereas a more detailed code relating a specific $\mathbf{s}$ to ISI, although likely being more information-rich, could be overly cumbersome and require temporal specificity that is beyond the capacity of any reasonable decoder. Further, the exact quantization proposed here and in our companion paper (Oswald et al. 2007) may be suboptimal as we have not used techniques based on rate distortion theory to motivate our quantization (Cover and Thomas 1991; Dimitrov and Miller 2001; Dimitrov et al. 2003). However, the purpose of $I(S,R)$ is not to achieve optimal estimates of the information capacity of the interval code, yet to be a reasonable measure of interval coding as internal parameters, such as DAC amplitude, are varied (see Figs. 7 and 8). We expect the qualitative conclusions drawn from using our quantization, and thereby $I(R,S)$ will be consistent with those gained from other quantization schemes.

RESULTS

Simple LIF-DAP bursting model

ELL pyramidal cells exhibit a complex burst dynamic in response to static depolarizing inputs (Lemon and Turner 2000; Turner et al. 1994). Within a single burst, an accelerated "ping-pong" interaction between somatic and dendritic excitability culminates with a high-frequency spike doublet. The second spike of the doublet is not followed by a dendritic spike, and consequently, the absence of a somatic DAP reveals a large burst afterhyperpolarization (bAHP). The bAHP signals the termination of the burst. In vitro experiments by Lemon and Turner (2000) distilled the burst mechanism to three general electrophysiological requirements. First, an active Na^+-dependent dendritic backpropagation is required to produce a DAP in the somatic membrane immediately after a somatic spike. Second, a spike frequency-dependent broadening of DAPs is needed to potentiate the DAPs thereby accelerating the burst frequency toward the spike doublet. The final requirement is a longer dendritic Na^+ channel refractory period compared with somatic Na^+ that leads to dendritic spike failure post the somatic spike doublet. This detailed characterization permitted the construction of several mathematical models of these cells, ranging from detailed multicompartmental models (Doiron et al. 2001, 2003) to two-compartment models (Doiron et al. 2002; Fernandez et al. 2005; Oswald et al. 2004) and phenomenological LIF-type bursting models (Noonan et al. 2003).

The response of an in vitro ELL pyramidal cell to low-frequency (0–10 Hz) random inputs showed burst signatures associated with the response to static stimuli, specifically multiple spike bursts with a decreasing ISI pattern and terminating bAHP (Fig. 2*A*). In contrast, the response of the same cell to broadband stimulus (0–60 Hz) lacked bursts with more than three spikes, typically only showing two spike bursts (Fig. 2*B*)—a behavior consistent with in vivo spike bursts collected during broadband stimulation (Gabbiani et al. 1996; Oswald et al. 2004). Furthermore, bAHPs marking the termination of a burst were absent in all recordings ($n = 52$). The lack of multi-spike bursts with decreasing ISIs and a terminating bAHP suggested that the ionic mechanisms responsible for these burst characteristics were not recruited during broadband stimulation.

In the APPENDIX, we present a phenomenological LIF-style model that contains the essence of the three mechanistic requirements of the full burst response to static inputs. This model reproduced the preceding experimental scenario, namely a full burst was observed in response to low-frequency inputs and only spike doublet bursts in response to broadband stimulation. The model response showed that the variables associated with slow DAP potentiation and dendritic refractory

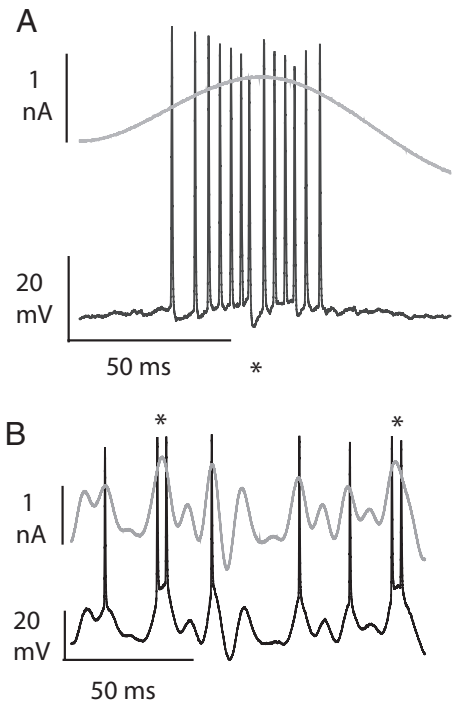

FIG. 2. Low-frequency and broadband stimulation in vitro. *A*: typical membrane response to 0- to 10-Hz Gaussian stimulus. Two bursts are observed with the 1st showing a clear decrease of the interspike interval (ISI) within the burst terminating with a high-frequency doublet and large burst afterpolarization (bAHP) (marked with an asterisk). *B*: typical membrane response to 0- to 60-Hz Gaussian stimulus. A mixture of isolated spikes and 2 spike bursts are observed. There is a lack of bAHP signatures signaling a specific cellular termination of the bursts.

period play a limited role in determining the neural response to broadband stimuli. Burst termination in this case was induced by the stimulus rapidly decreasing to negative values rather than an intrinsic ionic event. This suggested that a reduced LIF model with a history-independent DAP mechanism could model the ELL pyramidal cell response to broadband stimuli.

Thus motivated, we proposed an LIF-DAP model to replicate the spike train response of ELL pyramidal neurons driven by broadband stimuli (see METHODS). Briefly, the model is an LIF neuron that receives a dendro-somatic current (DAC) 2 ms after each spike reset. The DAC elicits a DAP response in the somatic membrane. Importantly, and unlike all other ELL burst models, the DAP is invariant with respect to past spiking history, meaning that the DAP neither potentiates during a burst nor fails after a somatic spike doublet. This model thus retains the effect of dendritic backprogation but ignores the second and third components of the classic ELL burst mechanism (Lemon and Turner 2000). The history independence of the post spike response makes this model a specific example of a broad class of spiking cell models called spike-response models (Gerstner and Kistler 2002). Similar style models have been successfully used to quantitative model spike behavior of both retinal ganglion cells (Pillow et al. 2005) as well as detailed models of cortical pyramidal neurons (Jolivet et al. 2004).

In response to broadband (0–60 Hz) Gaussian stimuli, the model neuron produced a sequence of single spikes and bursts along with a resultant DAC (Fig. 3*A*). With a reasonable choice of model parameters, the spike train firing rate was ~24 Hz, the burst fraction was 0.46 (number of spikes within bursts divided by the total number of spikes), and the burst event fraction was 0.20 (number of bursts divided by the total number of events, i.e., isolated spikes and bursts). These values are within the experimental range reported for the stimulus contrast of 1.4 nA (Oswald et al. 2006; Table 1).

The spike train autocorrelation $Q(\tau)$ (see METHODS) was compared between experiment (Fig. 3*B*), a standard LIF model (Fig. 3*C,* gray), and the LIF-DAP model (Fig. 3*C,* black). Both the experiments and the LIF-DAP model showed prominent high spike likelihood between 5 and 10 ms after a spike. This tendency was greatly reduced in the LIF model spike train. Additionally, the experimental ISI distribution (Fig. 3*D*) was also better matched with the LIF-DAP model (Fig. 3*E,* black) as compared with the LIF model (Fig. 3*E,* gray). Both the data and the LIF-DAP model ISI distributions showed a strong bimodality, yet the standard LIF model spike train had an ISI distribution with a weak bimodality similar to the one obtained under TTX blockade of dendritic Na^+ during presentations of broadband stimuli (Oswald et al. 2004). There were no significant ISI serial correlations in either the data or model outputs, marking them all as renewal spike trains (Gabbiani and Koch 1998).

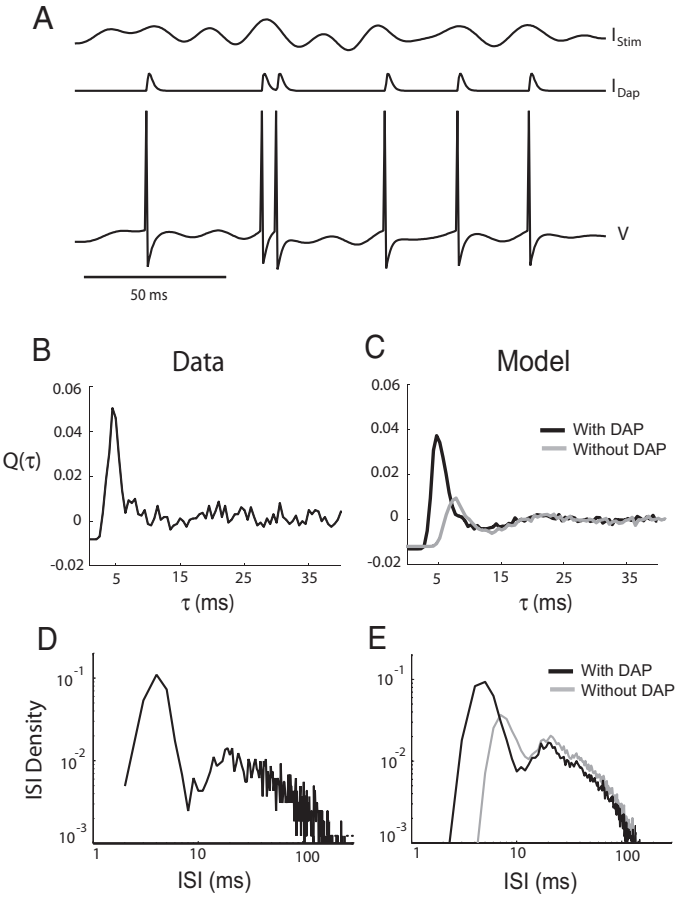

FIG. 3. LIF-DAP model spike train statistics. *A*: broadband Gaussian stimulus $I_{stim}(t)$ was given to the model cell (*top*). Each time the membrane V crosses threshold, the membrane is reset and a DAC input is given to the model (*middle*). The resultant model spike train is a combination of single spikes and bursts of spikes (*bottom*). *B*: autocorrelation $Q(\tau)$ for a typical spike train of an electrosensory lateral line lobe (ELL) pyramidal cell (*left*) and the model cell (*right*). *C*: ISI distribution for the experimental spike train in *B* (*left*) and the model cell (*right*). In both *B* and *C,* the model cell is shown when $A = 0.855$ nA (with DAP) and $A = 0$ (without DAP).

The quantitative fits of the LIF-DAP model to experimental results as well as the spike and burst firing rates were obtained by varying only a few model parameters. We varied the DAC amplitude (A), the mean input bias (b), and the stimulus contrast (σ). The other parameters, such as DAC time scale (α), DAC delay (τ_{DAC}), and the membrane timescale (τ_m), were fixed to fit experimentally estimated DAPs (see METHODS). With LIF-DAP parameters chosen to quantitatively match experimental data, we next compared the coding capabilities of the LIF-DAP model with those of real ELL pyramidal neurons.

LIF-DAP coding of dynamic inputs

In Oswald et al. (2004), a parallel processing scheme was introduced where isolated spikes and bursts respectively code the high- and low-frequency components of broadband input. Analogous to our past study we similarly analyzed the spike output of the LIF-DAP model. We computed the spectral coherence ($C(f)$; see METHODS) between the stimulus and the full spike train (Fig. 4*A,* black), the isolated spike train (Fig. 4*A,* dashed), and the burst train (Fig. 4*A,* gray). Satisfyingly, a clear streaming of low-frequency coding by bursts and high-frequency coding by isolated spikes is observed, identical to the results in Oswald et al. (2004).

Gabbiani et al. (1996) have shown that in vivo ELL pyramidal cell bursts outperform isolated spikes in detecting specific stimulus features; this was later replicated in vitro (Oswald et al. 2004). With the LIF-DAP model, we computed receiver operator curves (ROCs) comparing the selectivity of bursts (Fig. 4*B,* gray) and isolated spikes (Fig. 4*B,* dashed) reverse correlations with that of null reverse correlation (see Gabbiani et al.1996; Metzner et al. 1998; Oswald et al. 2004). Similar to experimental results, and a conductance based bursting model, the bursts demonstrated enhanced stimulus selectivity over isolated spikes (Oswald et al. 2004).

Finally our companion study Oswald et al. (2007) introduced an interval code whereby upstrokes of different amplitudes and slopes could reliability be discriminated based on two spike bursts of different ISI durations. With the LIF-DAP model, we computed both the average discriminability I_D and the interval code measure I_C for a range of ISI partition lengths T (Fig. 4, *C* and *D*). For ease of comparison, we also computed both the average response over the full data set from Oswald et al. (2006) and the LIF model ($A = 0$). The LIF-DAP model quantitatively matched the experimental results (Fig. 4, *C* and *D*), whereas the standard LIF model could not match I_C due to the lack of high-frequency burst intervals (see Fig. 3*B*).

In total, the preceding results show how the LIF-DAP model is sufficient to accomplish a wide variety of complex single neuron coding schemes that are exhibited by real in vitro and in vivo ELL pyramidal neurons. Furthermore, the fact that a basic LIF model could neither match the spike train statistics (Fig. 2) nor the spike train coding (Fig. 3) suggests that the LIF-DAP model is an appropriate minimal model of an ELL pyramidal cell in response to broadband inputs. We next used the LIF-DAP model to investigate a simplification of the interval code (Oswald et al. 2007) and describe the DAP dependence of interval coding.

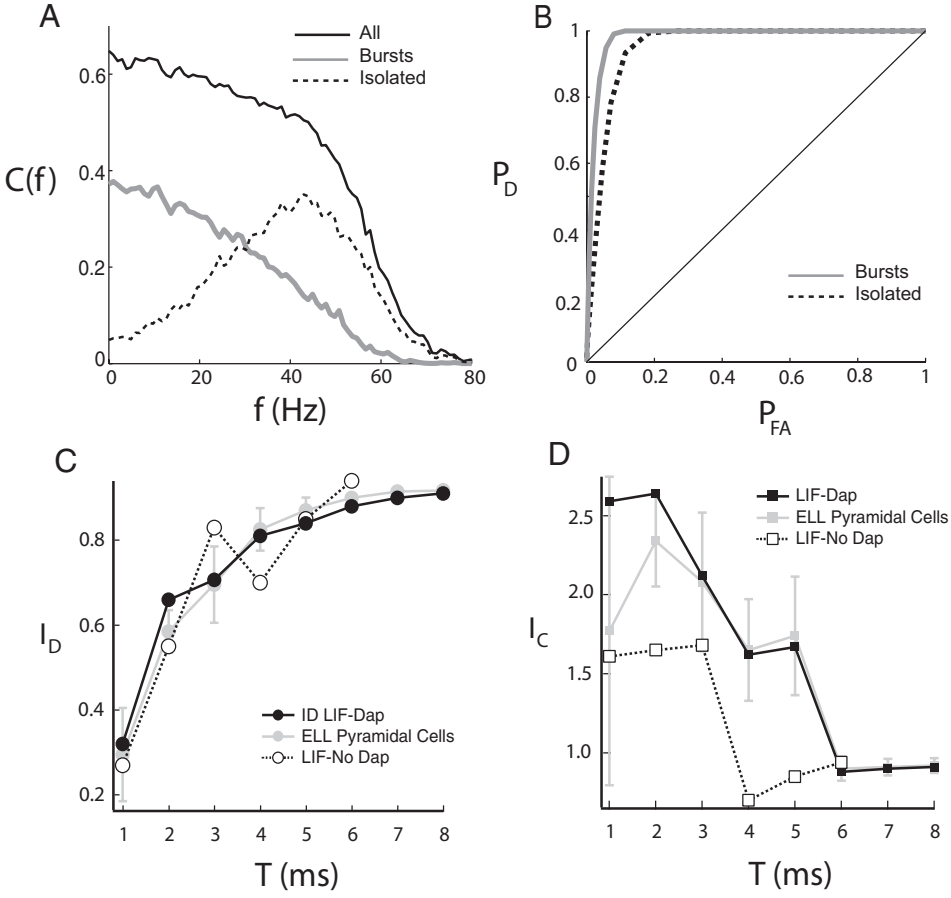

FIG. 4. LIF-DAP model coding performance. *A*: spectral coherence $C(f)$ between the stimulus and the full spike train (black), the isolated spike train (dashed), and the burst train (gray). *B*: receiver operator characteristic of the isolated spike train (dashed) and the burst train (gray). Both curves were computed for the respective spike trains as compared with the null event distribution. *C* and *D*: average burst ISI discriminability I_D and the interval code I_C as a function of ISI group duration T computed for the LIF-DAP model (black symbols), LIF model (open symbols), and the data set presented in Oswald et al. (2007) (gray symbols). The DAC amplitude A is as in Fig. 2.

Scale-ISI code

A major obstacle in any measure spike train coding is the reduction of stimulus dimension (Arcas and Fairhall 2003; Brenner et al. 2000; Metzner et al. 1998; Dimitrov and Miller 2001; Dimitrov et al. 2003; Rieke et al. 1997). In our companion study (Oswald et al. 2007), we projected burst triggered stimuli on suitably defined feature vectors to give a one-dimensional representation of the stimuli that elicit a specific burst. The feature vector was chosen to maximize the discriminability between two distinct interval groups. We then used a set of linear classifiers to quantify the performance of the burst interval code. The classifiers assessed both the ability of an ISI group to code a preferred feature and the difference between the features coded by distinct ISI groups. However, feature-extraction techniques do not allow for an intuitive picture of what are these actual differences and a visual inspection of the event triggered averages is required (see METHODS). In this section, we introduce a stimulus representation that significantly simplifies the interval code. This permits a computation of the mutual information between the burst intervals and the stimulus.

We considered the burst triggered average computed from all bursts, $\mathbf{s}_{all}$, with each stimulus vector $\mathbf{s}$ beginning at the first spike of the burst doublet and ending at the second spike. The maximal ISI over which the stimulus is defined was ~11 ms, whereas the fastest frequency component in I_{stim} had a period of 16 ms. This resulted in the observation that any burst triggered $\mathbf{s}$ (and by extension $\mathbf{s}_{all}$) was a smooth function with at most one maxima (see Fig. 3*A* in Oswald et al. 2007). We proposed the following reduction: each burst triggered reverse correlation, $\mathbf{s}$, was approximated by a scaled version of $\mathbf{s}_{all}$, making $\mathbf{s}_{all}$ an effective basis vector for the burst stimulus selectivity (see METHODS). To illustrate, we show four bursts from an ELL pyramidal cell, each of various interval lengths. For each burst, we show the stimulus waveforms $\mathbf{s}$ that elicited them (Fig. 5*A*, colored solid traces), $\mathbf{s}_{all}$ (black solid trace), and finally the best fit $\kappa\mathbf{s}_{all}$ (colored dotted lines). To quantify the success of the fit, we computed the χ^2 values of the one parameter fit between $\kappa\mathbf{s}_{all}$ and s for each burst in the data set (Fig. 5*B*). The fits were acceptable ($\chi^2 < 1$) for bursts that were less than ~10 ms, yet when the burst ISI approaches the time scales contained in the stimulus, the fit is less accurate. Satisfied with the reduction of stimulus dimension from a vector $\mathbf{s}$ to the scalar κ and basis upstroke $\mathbf{s}_{all}$, we represented both the stimulus and response as one dimensional quantities, i.e., a burst ISI and a scale parameter κ.

We observed a strong correlation between the ISI and κ in both the data (Fig. 5*C1*) and the model (Fig. 5*C2*). By quantizing the ISIs into four response groups (R_1–R_4, see METHODS) we defined the conditional stimulus distributions $P(\kappa|R_i)$ (colored groups in Fig. 5). For both the data and the LIF-DAP model, the distributions $P(\kappa|R_i)$ were unimodal and were easily visually discriminated (Fig. 5*D, 1* and *2*). The high-frequency ISI group (R_1) was most easily discriminated from the remaining lower frequency groups because the stimuli that elicit burst events in R_1 have the largest range in stimulus energy. This stimulus reduction strategy should be compared with the reduction of stimulus waveforms to either the average stimulus amplitude or rough stimulus slope estimate proposed in our companion paper (Oswald et al. 2007 Figs. 2, 3, and 5). A change in κ synthesizes both a change in stimulus amplitude and slope, is an equally intuitive reduction, and is a single scalar quantity making it amenable for further analysis (see following text).

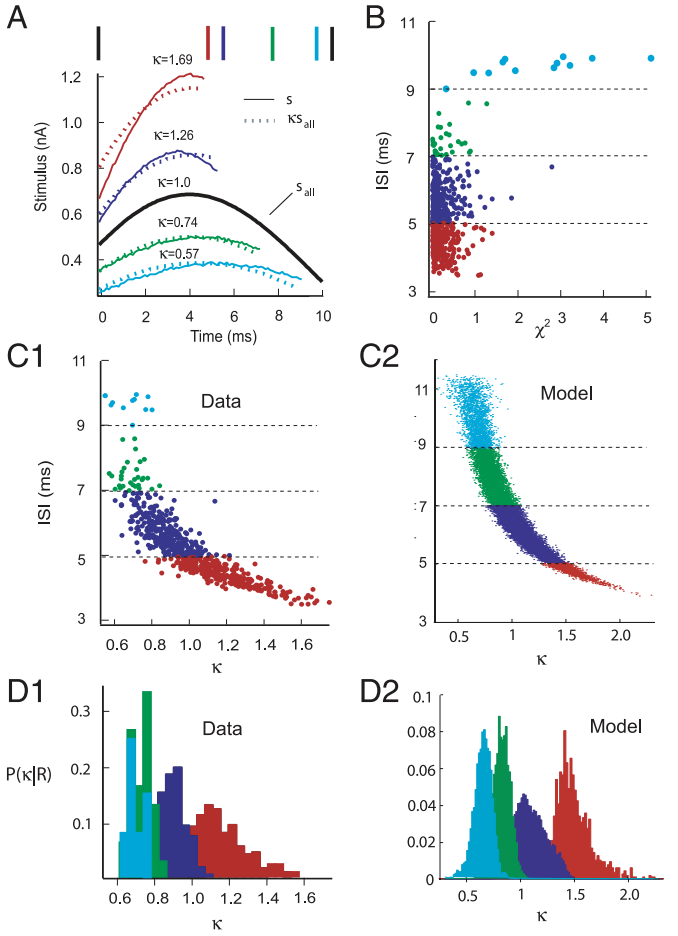

FIG. 5. Burst ISI codes for the scale of stimulus upstroke. *A*: full burst triggered average $\mathbf{s}_{all}$ (black) from a representative data set in Oswald et al. (2007). Representative ISI from each response group (R_i) with the stimulus $\mathbf{s}$ that triggered it (solid lines; cyan: R_4; green: R_3; blue: R_2; red: R_1). Plotted with $\mathbf{s}$ is $\kappa\mathbf{s}_{all}$ (dotted) where κ is the best fit scaling factor for each burst ISI and $\mathbf{s}_{all}$ is the full burst triggered average. *B*: χ^2 values for the best scale κ fits for all burst ISIs of a representative data spike train. Color codes are as given in *A*. *C*: computed scale κ as a function of burst ISI for the data set (*C1*) and the LIF-DAP model (*C2*). *D*: κ probability distributions condition on the ISI response group estimated from both the data (*D1*) and the LIF-DAP model (*D2*). The distribution bin size was 0.05 for the data and 0.005 for the model; each distribution is normalized so the area is 1. Colors are as marked in *A*. The DAC amplitude *A* is as in Fig. 2.

Given the conditional distributions $P(\kappa|R_i)$ and assuming a linear classifier model (see METHODS), we computed the probability of correct detection (P_D), the probability of false alarm (P_{FA}), and the classification error probability (ε). We compared ε_κ computed using our scale reduction (κ) of spike-triggered stimuli to the error probability ε_{FE} computed where stimulus reduction was performed using standard feature extraction techniques (Fig. 6*A*). When response groups are partitioned using 2-ms ISI intervals, a good quantitative agreement between the two reductions techniques is observed for discrimination between groups R_1/R_2 and R_2/R_3, whereas the agreement is fair for R_3/R_4. In particular, the optimal linear classifiers as defined by the minimum of the error probability

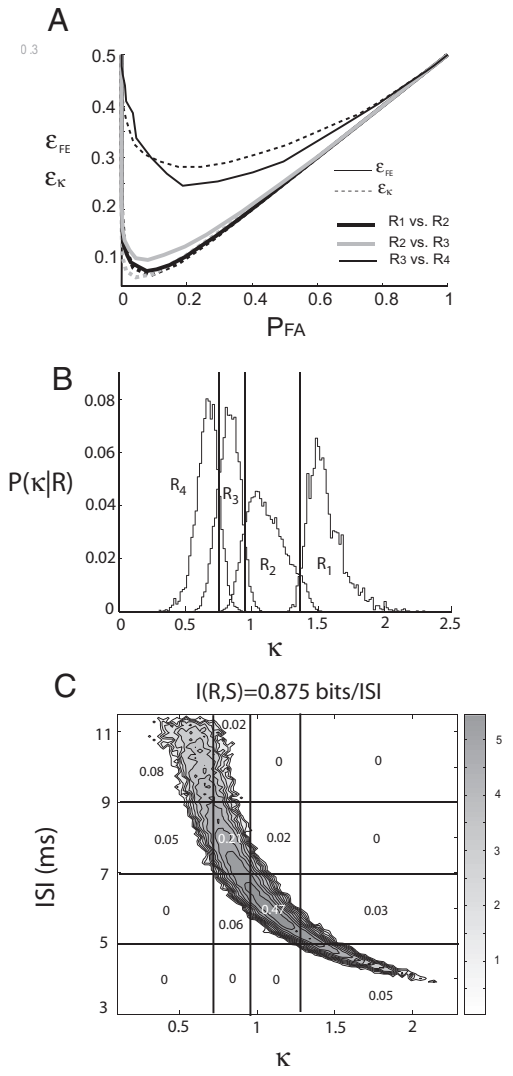

FIG. 6. Partitioned stimulus (S) and response (R). A: error probability curves computed using the full feature extraction method (ε_{FE}) and the simplified scale method (ε_{κ}) for the LIF-DAP model spike train. B: optimal partitioning of the upstroke scale κ determined by the minimums of the error probability curves. C: estimated joint distribution $P(\kappa,\text{ISI})$ and overlaid is the 16 state discrete joint distribution $P(S,R)$ obtained from the partitioning in B. The numbers in the partitioned κ-ISI space are the values of $P(S,R)$. The DAC amplitude A is as in Fig. 2.

are similar between the two stimulus reduction techniques. By locating the minimum of ε, we computed optimal thresholds κ_{12}, κ_{23}, and κ_{34} so as to best quantize the upstroke scale κ into well-defined stimulus groups S_1–S_4 (Fig. 6*B*, see METHODS). By partitioning both the stimulus (S_1–S_4) and the response (R_1–R_4), we computed the 16 state joint probability density $P(S,R)$ and overlaid the grid matrix on top of the continuum joint density $P(\kappa,\text{ISI})$ (Fig. 6*C*). The tendency for $P(S,R)$ to be centered along the diagonal of the $P(S,R)$ grid is evident. With an accurate estimation of $P(S,R)$, we computed the mutual information $I(S,R)$ between S and R (see METHODS). For the fitted parameters, the LIF-DAP model yielded an $I(S,R) = 0.875$ bits. With an upper bound of 2 bits (4 stimulus/response states), the interval code thus performs adequately, and these results further suggest that interval coding is a viable coding option for ELL pyramidal neurons.

Equipped with a quantitative measure of interval coding, we next evaluate the influence of dendritic excitability on interval coding.

Influence of DAP amplitude on interval coding

Several experimental studies have shown that the DAC amplitude (A) can be regulated through both expression of dendritic potassium channels (Noonan et al. 2003) or shunting inhibitory input to the proximal dendritic shaft (Mehaffy et al. 2005). Motivated by the capacity for DAP regulation, we computed the response entropy $H(R)$, the noise entropy $H(R|S)$, and the mutual information $I(S,R)$ [i.e., the difference between $H(R)$ and $H(R|S)$] for the LIF-DAP model as a function of the DAC amplitude A (Fig. 7*A*). Interestingly, both $H(R)$ and $I(S,R)$ show broad maxima, and all three measures decrease rapidly as A goes beyond ~1.3 nA. To identify the cause for the maximum, we studied the full joint density $P(\text{ISI},\kappa)$ and overlaid on top the optimal ISI-κ partition grid and the resulting joint density $P(S,R)$ for three values of A (Fig. 7, *B–D*). For small DAC amplitudes (Fig. 7*B*), the probability of observing high-frequency burst ISIs was negligible and the partitioning ranged over only S_2–S_4 and R_2–R_4, thereby limiting $H(S,R)$ and by extension $I(S,R)$. In a similar fashion, when the DAP amplitude was large (Fig. 7*D*), the burst response was dictated by the DAP alone and the partitioning was dominated by S_1 and R_1, severely restricting the information $I(S,R)$. Only when the DAC amplitude A was moderate (Fig. 7*C*) could a full spanning of the response groups R_1–R_4 be achieved. This full spanning allowed the response entropy $H(R)$ to be large, yet the DAP amplitude was not so overpowering as to eliminate the stimulus dependence of the response, hence permitting a small noise entropy $H(R|S)$. This combination lead to a maximum in $I(S,R)$.

The probability of a burst ISI increases with the DAC amplitude A (see Fig. 3*E*). This resulted in the burst frequency f_{burst} (average number of bursts per second) also increasing with A (Fig. 8*A*, thin black line). As a consequence, the information rate, $I_{\text{rate}}(S;R) = f_{\text{burst}}\text{I}(S,R)$, of the interval code showed a clear maximum as a function of A (Fig. 8*A*, thick black line). This again resulted from a moderate DAC amplitude permitting a wide range of possible responses (as in Fig. 7); indeed the maximums of the $I(S;R)$ and $I_{\text{rate}}(S;R)$ approximately coincided. The combination of these results show that although the DAP is required to elicit a burst response, the DAC enters the spike generation zone (V) as a current so its influence must be moderate to allow the stimulus I_{stim} to effectively influence the burst response.

The preceding results were conditional on the stimulus I_{stim} having a fixed contrast σ. However, it is expected in a natural environment that the contrast of electric field modulations can vary significantly. We computed the $A - I_{\text{rate}}(S;R)$ curve for five different stimulus contrasts and observed a systematic shift of the maximum information rate to lower DAP amplitudes as contrast increases (Fig. 8*B*). The pairing of the optimal A for a given σ was such that if σ increased, the DAP mechanism needed to decrease. Otherwise the combination of a strong stimulus and a large DAP would evoke bursts leading to the scenario featured in Fig. 7*D*: the majority of bursts fall into ISI group R_1. In the opposite scenario, when the stimulus contrast was weak, the DAP amplitude was required to be large to

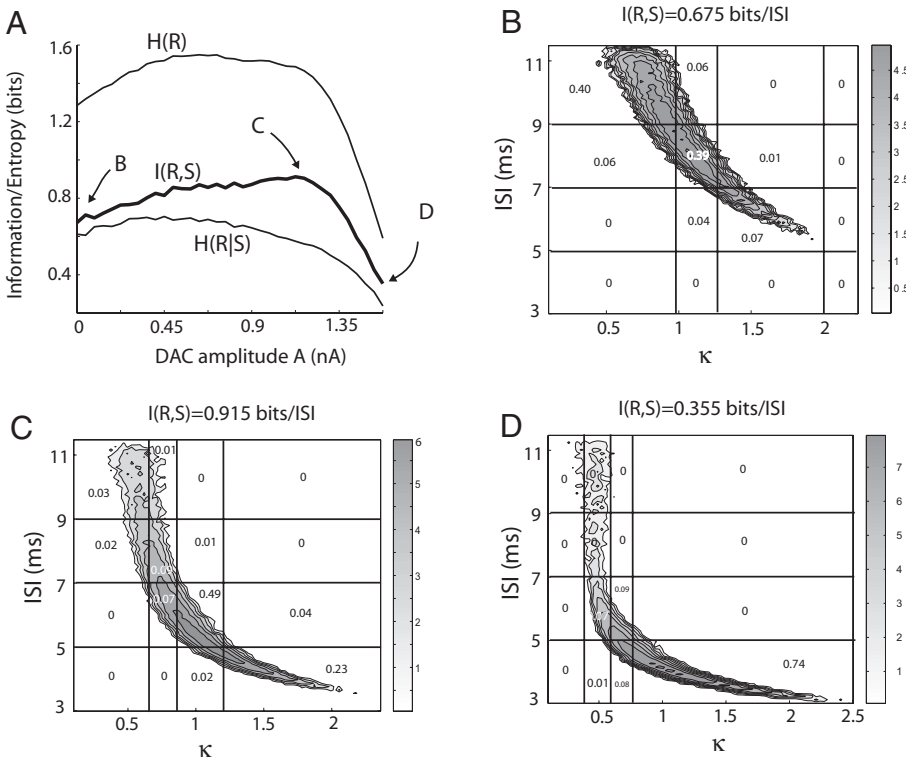

FIG. 7. $I(S,R)$ is maximized for the LIF-DAP model at an intermediate DAP amplitude. *A*: response entropy $H(R)$, noise entropy $H(R|S)$, and the mutual information $I(S,R)$ computed from the partitioned stimulus and response are plotted as a function of the DAC amplitude *A*. A broad maximum is seen in $I(S,R)$. *B*: $P(\kappa,\text{ISI})$ and $P(S,R)$ when the DAP amplitude is 0. *C*: $P(\kappa,\text{ISI})$ and $P(S,R)$ when *A* is such that $I(S,R)$ is maximized. *D*: $P(\kappa,\text{ISI})$ and $P(S,R)$ when *A* is large and $I(S,R)$ is small.

ensure burst responses, else only the scenario in Fig. 7*B* occurred: the majority of bursts fall into ISI groups R_3–R_4.

DISCUSSION

In this paper, we have shown that the burst response of ELL pyramidal cells to broadband dynamic inputs does not require the ionic machinery necessary to account for the burst response to static or low-frequency inputs. We introduced a simple LIF-DAP model that was successful at reproducing the output statistics of both the spike train and ISI sequences of in vitro ELL pyramidal cells stimulated with broadband inputs. The LIF-DAP model could also mimic the parallel processing code (Oswald et al. 2004), enhanced selectivity of burst responses as compared with isolated spikes (Gabbiani et al. 1996), and interval coding (Oswald et al. 2007) associated with these cells. We used the LIF-DAP model to investigate a stimulus dimension reduction assumption where the burst-triggered reverse correlation of a specific burst was approximated as a scaled version of the average burst triggered stimulus. The scale parameter (κ) is an effective one dimensional representation of the stimulus that drives a given burst ISI. Following our companion paper (Oswald et al. 2007), we used a set of linear classifiers to motivate a quantization of the stimulus and response groups yielding a scale-ISI code for the ELL burst response. The ISI response was shown to carry maximal information about the upstroke scale when the DAP size was moderate. Finally, the optimal DAP size was dependent on the contrast (or variance) of the stimulus such that when the contrast was large the optimal DAP value was small and vice versa. In summary, reducing both the biophysics of bursting ELL pyramidal cells and the quantification of the putative interval code suggested a simple neural code, of which the core biophysical components, DAPs, are widespread.

Caricature of the DAP-dependent interval code

In this section, we use the simplicity of the LIF-DAP model to present a caricature that highlights the essence of several ELL burst coding strategies (Oswald et al. 2004, 2007) (Figs. 5–8 of this paper). To ease the analysis in what follows, we replace the Gaussian stochastic process $I_{\text{stim}}(t)$ with a sinusoidal forcing $I_{\text{stim}}(t) = A_{\sin} \sin(2\pi \text{ft})$. We begin with a straightforward presentation of the parallel processing performed by burst and isolated spikes (Fig. 4).

The burst response to a low-frequency input (20 Hz, Fig. 9*A, top*) occurs due to a temporally coincident depolarizing stimulus (Fig. 9*A, middle*) and DAC from the first spike of the burst (Fig. 9*A, bottom*). The combination of these two input events elicits the second spike of the burst. In contrast, when the stimulus is high-frequency (50 Hz) then the DAC from the first spike of the burst is now coincident with the hyperpolarizing downstroke of the dynamic stimulus (Fig. 9*B, middle* and *bottom*). In this scenario, the DAC is insufficient to produce a second spike, and there is only a single isolated spike in response (Fig. 9*B, top*). Thus bursts are associated with the low-frequency components of a dynamic stimulus, whereas isolated spikes are associated with high-frequency components— facilitating a parallel processing of dynamic inputs (Oswald et al. 2004).

Using the LIF-DAP model, we can summarize the interval code proposed in our companion paper (Oswald et al. 2007). When a stimulus upstroke is both shallow in amplitude and slope or equivalently has a small-scale parameter κ (Fig. 9*C, middle,* black curve), then the combination of the DAC of the first spike (Fig. 9*C, bottom,* black curve) and the stimulus produces a delayed second spike resulting in a long burst ISI response (Fig. 9*C, top,* black curve). On the other hand, if the upstroke has a large amplitude and steep slope, i.e., a large κ

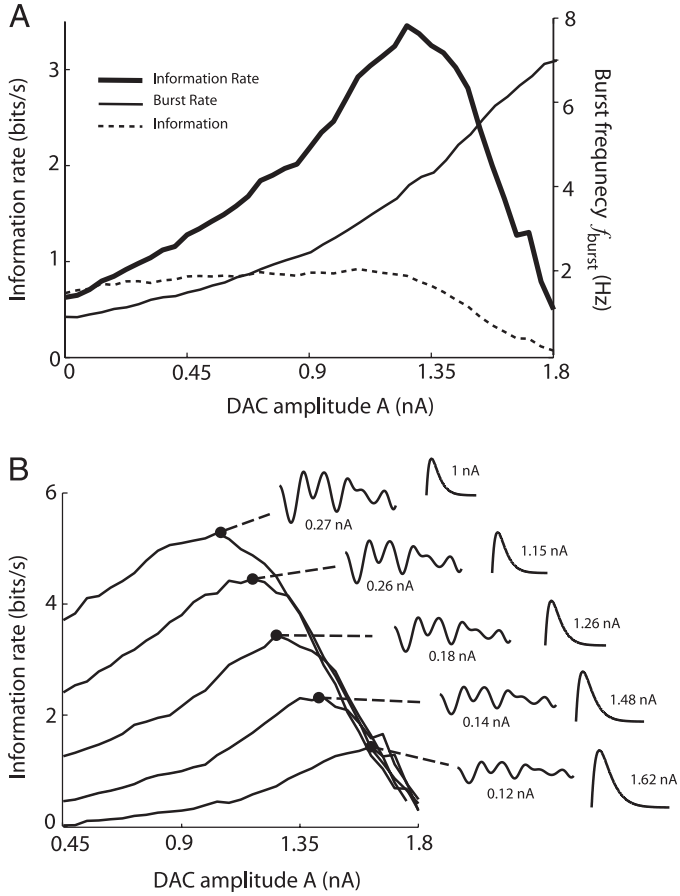

FIG. 8. $I_{rate}(S,R)$ is dependent on DAC amplitude (A) and stimulus contrast (σ). A: burst frequency f_{burst}, $I(S,R)$, and $I_{rate}(S,R) = f_{burst}\ I(S,R)$ are plotted as a function of the dendro-somatic current amplitude A for the LIF-DAP model. A distinct maximum is observed in $I_{rate}(S,R)$ at an intermediate DAC amplitude. B: $I_{rate}(S,R)$—a curve computed for 5 different stimulus contrast values. *Insets*: contrast of the stimulus and the value of A that maximizes $I_{rate}(S,R)$. Note here the maximum of $I_{rate}(S,R)$ shifts to smaller DAC amplitudes with and increases in σ.

(Fig. 9*C, middle,* red curve), then the DAC of the first spike (Fig. 9*C, bottom,* red) and the stimulus combine to produce a rapid second spike and a short burst ISI (Fig. 9*C, top,* red trace). Thus the length of a burst ISI and the upstroke scale κ are inversely related, yielding the essence of our interval code. Finally, given a fixed stimulus amplitude and a variable DAC amplitude similar arguments can be made to ground the observation the DAC amplitude can affect the burst response and hence the interval code (Fig. 9*D*).

Although all of these arguments for the mechanistic basis of the parallel processing and interval codes are simple, they do require a neural model that does not contain the ionic complexities of previous ELL models (Doiron et al. 2001–2003; Fernandez et al. 2005; Noonan et al. 2003). Using these more biophysically realistic models does not allow a dissection of burst response into a combination of the stimulus and a *history-independent* DAP; rather a far more cumbersome, and possibly intractable, treatment would be needed. The other significant advantage of motivating ELL coding strategies with the LIF-DAP model rather than more realistic models is that the ionic features of real ELL pyramidal cells that are ignored in the LIF-DAP model have not been observed in other types of neurons. Thus by framing the coding strategies employed by bursting ELL pyramidal neurons with the LIF-DAP framework, the potential applicability of these strategies to neurons in other brain regions is increased. Indeed, the basic DAP component of the LIF-DAP model has been well documented in both cortical (Larkum et al. 2004) and hippocampal (Magee and Carruth 1999) pyramidal cells as well as spinal cord motor neurons (Larkum et al. 1996), suggesting that the coding paradigms elucidated in the ELL may be operating in other brain regions.

Stimuli reduction and scale codes

The reduction of input stimuli and neural response to their essential features is an important component of any theory of neural processing. An increasingly popular representation of a spike train code is the spike/burst triggered reverse correlation (Reike et al. 1997). Principal component analysis or feature extraction techniques reduce the multi-dimensional stimuli measured with reverse correlation to a more manageable representation (Arcas and Fairhall 2003; Brenner et al. 2000; Metzner et al. 1998). However, a limitation of these techniques is that after reduction an intuitive interpretation of the stimuli that elicit a neuronal response is often lacking. This makes a straightforward explanation of a specific neural code sometimes difficult to obtain. For instance, our companion study (Oswald et al. 2007) as well as past studies of burst coding (Kepecs and Lismann 2003) used these or similar reduction techniques to quantify the stimulus selectivity of bursts with different characteristics (ISI length, number of spikes, etc.). However, although these techniques give a well-defined metric

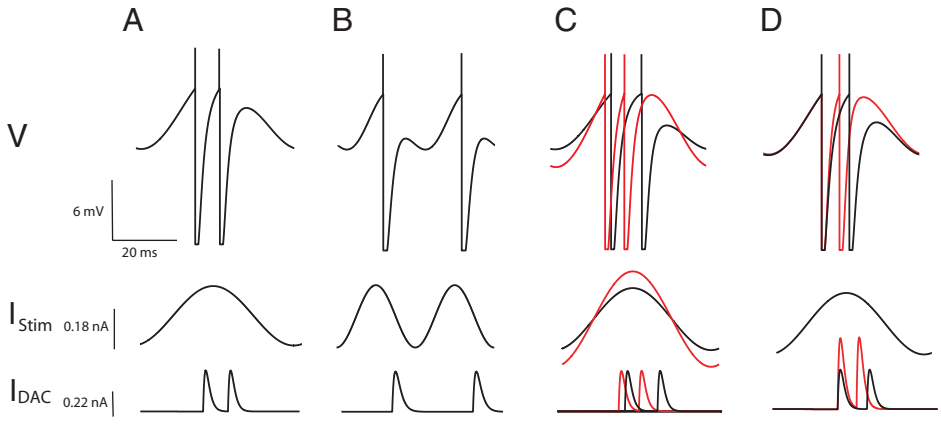

FIG. 9. Schematic illustration of LIF-DAP dynamics in ELL coding. A: burst (*top*) and associated DAP (*bottom*) responses to a suprathreshold (I_{sin} = 0.135 nA), low-frequency (f = 20 Hz) sinusoidal input (*middle*). B: isolated spike (*top*) and associated DAC (bottom) responses to a suprathreshold (I_{sin} = 0.135 nA), high-frequency (f = 50 Hz) sinusoidal input (*middle*). C: burst and associated DAC responses to large (I_{sin} = 0.18 nA, red curves) and moderate amplitude (I_{sin} = 0.135 nA, black curves) low-frequency (f = 20 Hz) sinusoidal input. D: burst and associated DAC responses to low-frequency (f = 20 Hz) sinusoidal input with the DAC amplitude set to moderate (A = 0.855 nA, black curve) and large (A = 1.22 nA, red curve) values.

to stimulus selectivity differences, one must visually compare the different response triggered averages to see what exactly those differences are.

The basis vector ($\mathbf{s}_{all}$) and the scale approximation (κ) gave an empirically justified reduction of the large dimensional stimulus patterns (mean triggered responses) to an effective one variable representation. The scale of an "upstroke" in a dynamic electrosensory scene might represent how close the fish is to prey during its hunting scans of the environment (Chen et al. 2005; Nelson and MacIver 1999; D. Babineau, A. Longtin, and J. E. Lewis, unpublished data). Further, even though the exact shape of the basis vector $\mathbf{s}_{all}$ is defined by the statistics of I_{stim}, the relation between κ and ISI may be preserved for a wide range of I_{stim} statistics, possibly even for non-Gaussian stimuli. One final advantage of the scale representation was that it permitted a partitioning of the stimulus space giving an estimate of the mutual information $I(S,R)$ of the interval code. Representing coding by the metric $I(S,R)$ allowed an analysis of how the interval code was influenced by neural biophysics, in this instance, the DAP generation mechanism.

In summary, the assumption of a basis upstroke and its scaling by κ synthesized the stimulus selectivity differences that shaped the feature vectors f_{ij} used in Oswald et al. (2007). We expect that similar intuitive stimulus reductions in other coding scenarios may provide a role for cellular properties distinct from the ones presented here.

Reduction of the ELL burst mechanism and natural electric fish prey capture

Most single-cell burst models can be analyzed with a decomposition of their dynamics into fast (spiking) and slow subsystems (see Izhikevich 2007; Rinzel and Ermentrout 1998). Often the evolutions of the fast and slow systems are coupled, i.e., the slow subsystem transitions the fast subsystem between spiking and quiescence behavior, and the time-averaged spiking dynamics drive the slow system's response. Such a fast-slow decomposition has been applied to models of bursting ELL pyramidal neurons when driven by static inputs (Doiron et al. 2002; Fernandez et al. 2005). In the APPENDIX, we show how the slow dynamics of a DAP potentiation and dynamic refractory period are effectively frozen when stimuli with fast timescales drive the cell membrane. This observation prompted the LIF-DAP model, which only has a fast system yet the response of which quantitatively matched to the output statistics and coding performance of real ELL pyramidal cells stimulated by broadband input. Despite the fact that we labeled the spike train output of the LIF-DAP model as bursting (see ISI histogram and spike autocorrelation in Fig. 3), the burst mechanism is quite distinct from those of fast-slow burst mechanisms because the burst termination could not be attributed to an ionic event but to a downstroke in the stimuli. The response of the LIF-DAP model to a static stimulus is a tonic spike discharge itself (not shown), indicating that the LIF-DAP model should not be classified as an intrinsic burst mechanism in the same category as many other intrinsic bursting models (Izhikevich 2007). The LIF-DAP model demonstrates that the temporal content of a driving stimulus can "gate" the influence of biophysical mechanisms on the spike/burst train output.

From a neuroethological perspective, the stimulus gating of burst responses described above can have intriguing electrosensory coding consequences. Nelson and MacIver (1999) illustrated the scanning motions used when, under laboratory conditions, single electric fish hunt for prey typically produce electrosensory signals with frequency components $<$20 Hz. However, when multiple fish (of both *A. leptorhynchus* and related species) are present, they will often forage in groups of several fish as well as in isolation (Tan et al. 2005; E. Fortune personal communication). Under these circumstances, the presence of conspecifics will produce beat frequencies that often exceed 30 Hz (E. Fortune, personal communication). There are therefore two scenarios for encoding the low-frequency signals that occur during prey detection and capture.

When hunting in isolation, these fish will receive only low-frequency signals that evoke the full burst mechanism as described in the preceding text (Fig. 2*A*). The large numbers of spikes that can occur during such a burst would presumably be a strong signal and readily decoded by higher brain centers. Although we have not specifically investigated this scenario, it is plausible that the firing rate during the long bursts evoked by such stimuli might simply code for the strength of the signal (Mehaffey et al. 2005). Modeling this scenario would require pyramidal cell models incorporating the full biophysical burst dynamics (Doiron et al. 2001, 2002; Fernandez et al. 2005; Lemon and Turner 2000).

In contrast, when foraging in groups high-frequency signals will also be present, and the full burst sequence will be disrupted by stimulus downstrokes as discussed in the preceding text. In this case, the LIF-DAP model of pyramidal cells would be appropriate, and the fish might resort to an interval code to assess the strength of the low-frequency prey signals. Clarification of these issues will require recording the responses of pyramidal cells and their midbrain targets to moving objects (simulating prey) in the absence or presence of high-frequency signals (mimicking conspecifics).

Consistent with these results is recent work in LGN where pyramidal cells were shown to significantly increase their burst probability when driven by natural scenes as compared with their response to broadband visual scenes (Lesica and Stanley 2004; Lesica et al. 2006). An analysis of the burst-triggered average indicated that the specific natural scenes had slow enough time scales so as to permit a prolonged hyperpolarization required by the burst mechanism characterized in the cells. In contrast, any high-frequency stimuli components, as found in white-noise visual scenes, removed the chance for long periods of hyperpolarization and hence disallowed burst outputs. An intriguing consequence is that a transition between tonic and burst codes may be mediated not only by the modulation of cellular processes or cortical feedback (Sherman 2001; Wang et al. 2006) but simply by the statistics of the stimuli that drive the neural response (Lesica et al. 2006).

APPENDIX

In this APPENDIX, we give an informal reduction of the full burst mechanism (Doiron et al. 2001–2003; Lemon and Turner 2000; Noonan et al. 2003) to the simple model introduced in METHODS. We first present a modified version of the LIF-type burst mechanism presented in Noonan et al. (2003). The model dynamics are described by the following system of differential equations

$$C\frac{dV}{dt} = b - gV + Ap(t - \tau_{DAP})x(t - \tau_{DAP}) + I_{stim}(t) \quad (A1)$$

$$\frac{dx}{dt} = y \quad (A2)$$

$$\frac{dy}{dt} = -\alpha^2 x - 2\alpha y + \alpha^2 \sum_m \delta(t - t_m)\theta(t - t_{m-1} - r) \quad (A3)$$

$$\tau_p \frac{dp}{dt} = p_x - p + Bp^2 \sum_m \delta(t - t_m)\theta(t - t_{m-1} - r) \quad (A4)$$

$$\tau_r \frac{dr}{dt} = r_\infty - r + C \sum_m \delta(t - t_m)\theta(t - t_{m-1} - r) \quad (A5)$$

The dynamic variables *V, x,* and *y*, as well as parameters *C, g, b,* α, and stimulus $I_{stim}(t)$ are identical to those presented in METHODS. The term *Apx* in the right-hand side of *Eq. A1* represents the DAC flow that occurs post a somatic spike. The DAC is scaled by the factor *Ap*, *A* is a static amplitude, and *p* is a nonlinear dynamic DAC potentiation critical for proper burst generation in the ELL as measured from static input scenarios (Lemon and Turner 2000). Finally, *r* is the dendritic spike refractory period that has also been shown to be dynamic (Noonan et al. 2003).

At almost every spike time t_i, we have that $p \rightarrow P + Bp^2$ and $r \rightarrow r + Cr$ in a discontinuous fashion. This rule was conditional on if $t - t_{i-1} > r$ or not; this was implemented by the Heaviside terms $\theta(t - t_{i-1} - r)$ in *Eqs. A3–A5* where $\theta(x) = 1$ if $x > 0$, otherwise $\theta(x) = 0$. If $t - t_{i-1} < r$, the dendritic Na^+ channels were considered to be refractory and dendritic spiking could not be initiated. This implied that *x* does not undergo a DAP excursion and *p* and *r* were not discontinuously updated. It should be mentioned that both τ_p and τ_r were slow variables that require a significant recruitment of activity that occurs with rapid and sustained spike discharge. The combination of the conditional spike updates and the dynamic refractory period gave the model described by *Eqs. A1–A5* the qualitative behavior of ELL pyramidal cell spike and burst discharge (see Noonan et al. 2003 for further model analysis).

When $I_{stim}(t)$ was Gaussian with a spectrum equally distributed between 0 and 10 Hz and 0 elsewhere, the model response (Fig. A1*A1*) was qualitatively similar to the experimental results (Fig. 2*A*). The multispike burst was characterized with a potentiating DAC (Fig. A1*A2*) and the bursts terminated with the refractory variable *r* surpassing the ISI value (Fig. A1*A3*). Indeed, a scatter plot of *r* against the ISI (*r* is measured at the time of the 2nd spike) shows that it is quite typical for *r* to grow larger than the ISI (Fig. A1*A4*). Additionally, a scatter plot of *p* against the ISI shows *p* increasing from 0.4 for

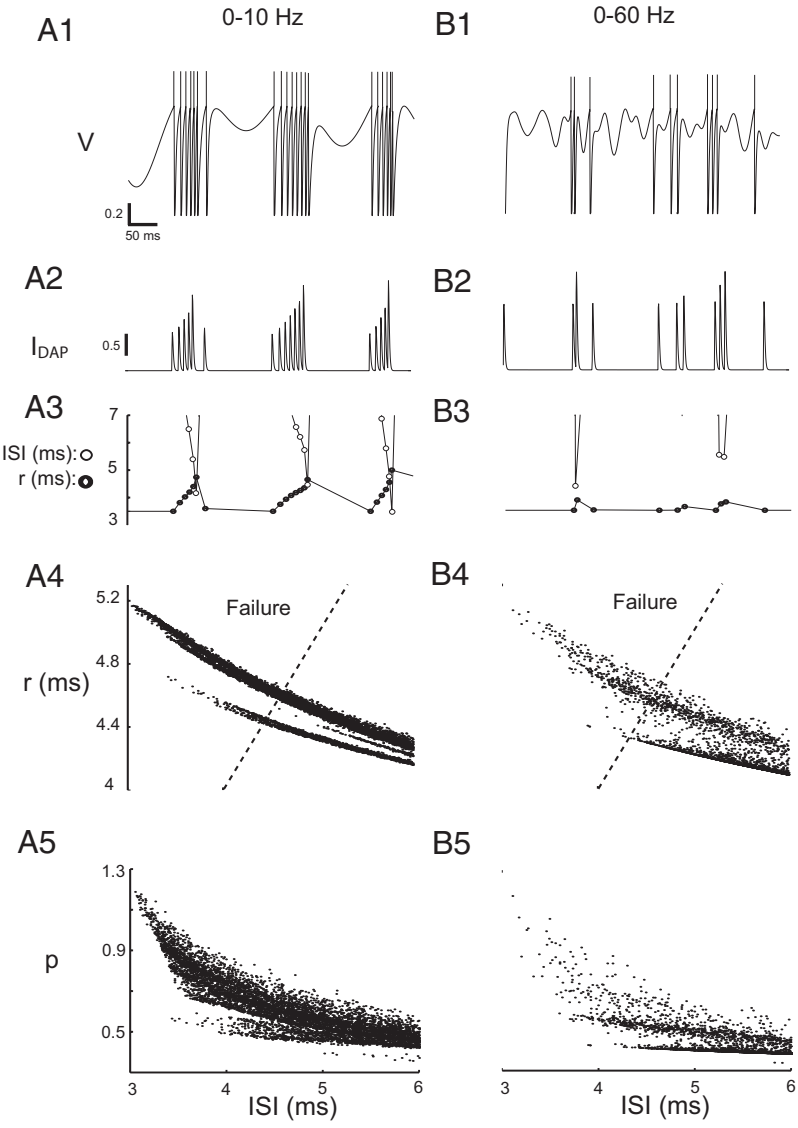

FIG. A1. Slow variables (DAC potentiation and dendritic refractory period) are required to reproduce the spike response to low-frequency stimulus 0–10 Hz but not broadband 0- to 60-Hz stimulus. *A1*: membrane *V* response to low-frequency inputs. *A2*: DAP potentiation *p* for the response in *A1*. *A3*: dendritic refractory period *r* for the response in *A1*. *A4*: scatter plot of *p* and ISI for 5,000 bursts. *A5*: scatter plot of *r* and ISI for the same bursts in *A4*. The dashed line is the unit diagonal marking the failure region for dendritic backpropagation. *B, 1–5*: identical to *A, 1–5,* except that the stimulus $I_{stim}(t)$ is broadband.

long ISIs to >1 for very short ISIs (Fig. A1*A5*), indicating significant DAP potentiation during a burst. Thus for low-frequency inputs, the burst models with slow DAP potentiation and a dynamic refractory variable that were developed to match experiments with static inputs were both necessary and sufficient to explain the experimental results in Fig. 2*A*.

When $I_{stim}(t)$ is Gaussian with a spectrum equally distributed between 0 and 60 Hz (and 0 elsewhere), the model response (Fig. A1*B1*) was qualitatively similar to the experimental results (Fig. 2*B*) and the LIF-DAP model (Fig. 3*A*). Critically, neither of the two slow variables r and p played a significant role in determining burst behavior. Specifically, the bursts were only very rarely terminated when r surpassed the ISI (Fig. A1*B, 3* and *5*), and the DAP potentiation was not as evident as the slow input case (Fig. A1*B2*) with p being restricted near 0.4 independent of the burst ISI (Fig. A1*B4*).

The results show in Fig. A1*B* suggests that although the dynamical variables r and p, and their associated *Eqs. A4* and *A5,* were required to replicate the experimental activity shown in Fig. 2*A,* they were not required to replicate the activity in Fig. 2*B.* Motivated by this, we remove *Eqs. A4* and *A5* and clamp p at 0.4 giving the simple LIF-DAP model presented in METHODS.

The model parameters were identical to those used in METHODS with the addition of $A = 2.14$ nA, $p_\infty = 0.4$, $r_\infty = 4$ ms, $B = 0.3$, $C = 0.4$ ms, $\tau_r = 5$ ms, $\tau_p = 5$ ms.

GRANTS

B. Doiron is a long term fellow of the Human Frontiers Science Program (HFSP-LT788).

REFERENCES

Agmon-Snir H, Carr CE, Rinzel J. The role of dendrites in auditory coincidence detection. *Nature* 393: 268–272, 1998.

Arcas B, Fairhall AL. What causes a neuron to spike? *Neural Comput* 15: 1789–1807, 2003.

Bastian J, Chacron MJ, Maler L. Receptive field organization determines pyramidal cell stimulus-encoding capability and spatial stimulus selectivity. *J Neurosci* 22: 4577–4590, 2002.

Berman NJ, Maler L. Neural architecture of the electrosensory lateral line lobe: adaptations for coincidence detection, a sensory searchlight and frequency-dependent adaptive filtering. *J Exp Biol* 202: 1243–1253, 1999.

Berman NJ, Plant J, Turner RW, Maler L. Excitatory amino acid transmission at a feedback pathway in the electrosensory system. *J Neurophysiol* 80: 3214–3232, 1997.

Brenner N, Bialek W, van Steveninck RD. Adaptive rescaling maximizes information transmission. *Neuron* 26: 695–702, 2000.

Cover TM, Thomas JA. Elements of Information Theory. New York: Wiley, 1991.

Chacron MJ, Doiron B, Maler L, Longtin A, Bastian J. Non-classical receptive field mediates switch in a sensory neuron's frequency tuning. *Nature* 423: 77–81, 2003.

Chacron MJ, Maler L, Bastian J. Electroreceptor neuron dynamics shape information transmission. *Nat Neurosci* 8: 673–678, 2005.

Chen L, House JL, Krahe R, Nelson ME. Modeling signal and background components of electrosensory scenes. *J Comp Physiol [A]* 191: 331–345, 2005.

Doiron B, Laing C, Longtin A, Maler L. Ghostbursting: a novel neuronal burst mechanism. *J Comput Neurosci* 12: 5–25, 2002.

Doiron B, Longtin A, Turner RW, Maler L. Model of gamma frequency burst discharge generated by conditional backpropagation. *J Neurophysiol* 86: 1523–1545, 2001.

Doiron B, Noonan L, Lemon N, Turner RW. Persistent Na^+ current modifies burst discharge by regulating conditional backpropagation of dendritic spikes. *J Neurophysiol* 89: 324–337, 2003.

Dimitrov AG, Miller JP. Neural coding and decoding: communication channels and quantization. *Network* 12: 441–472, 2001.

Dimitrov AG, Miller JP, Gedeon T, Aldworth Z, Parker AE. Analysis of neural coding through quantization with an information-based distortion measure. *Network.* 14: 151–176, 2003.

Duda RO, Hart PE, Stork DG. Pattern Classification (2nd ed.). New York: Wiley-Interscience, 2001.

Fernandez FR, Mehaffey WH, Turner RW. Dendritic Na^+ current inactivation can increase cell excitability by delaying a somatic depolarizing afterpotential. *J Neurophysiol* 94: 3836–3848, 2005.

Gabbiani F, Koch, C. Principles of spike train analysis. In: *Methods in Neuronal Modeling,* edited by Koch C, Segev, I. Cambridge, MA: MIT Press, 1998, p. 313–360.

Gabbiani F, Krapp HG, Koch C, Laurent G. Multiplicative computation in a visual neuron sensitive to looming, *Nature* 420: 320–324, 2002.

Gabbiani F, Metzner W, Wessel R, Koch C. From stimulus encoding to feature extraction in weakly electric fish. *Nature* 384: 564–567, 1996.

Gerstner W, Kistler W. Spiking Neuron Models: Single Neurons, Populations, and Plasticity. Cambridge, UK: Cambride Univ. Press, 2002.

Izhikevich EM. Dynamical Systems in Neuroscience: The Geometry of Excitability and Bursting. Cambridge, MA: MIT Press, 2007.

Jolivet R, Lewis TJ, Gerstner W. Generalized integrate-and-fire models of neuronal activity approximate spike trains of a detailed model to a high degree of accuracy. *J Neurophysiol* 92: 959–976, 2004.

Kepecs A, Lisman J. Information encoding and computation with spikes and bursts. *Network Comput Neural Syst* 14: 103–118, 2003.

Koch C, Segev I. The role of single neurons in information processing. *Nat Neurosci* 3: 1171–1177, 2000.

Krahe R, Gabbiani F. Burst firing in sensory systems. *Nat Neurosci* 5: 13–23, 2004.

Laing CR, Coombes S. Mode locking in a periodically forced "ghostbursting" neuron model. *Int J Bifurcations Chaos* 15: 1433–1444, 2005.

Laing CR, Doiron B, Longtin A, Noonan L, Turner RW, Maler L. Type 1 burst excitability. *J Comput Neurosci* 14: 329–342, 2003.

Laing CR, Longtin A. Periodic forcing of a model sensory neuron. *Phys Rev E* 67:051928, 2003.

Larkum ME, Rioult MG, Luscher HR. Propagation of action potentials in the dendrites of neurons from rat spinal cord slice cultures. *J Neurophysiol* 75: 154–170, 1996.

Larkum ME, Senn W, Luscher HR. Top-down dendritic input increases the gain of layer 5 pyramidal neurons. *Cereb Cortex* 14: 1059–1070, 2004.

Lemon N, Turner RW. Conditional spike backpropagation generates burst discharge in a sensory neuron. *J Neurophysiol* 84: 1519–1530, 2000.

Lesica NA, Stanley GB. Encoding of natural scene movies by tonic and burst spikes in the lateral geniculate nucleus. *J Neurosci.* 24: 10731–10740, 2004.

Lesica NA, Weng C, Jin J, Yeh CI, Alonso JM, Stanley GB. Dynamic encoding of natural luminance sequences by LGN bursts. *PLOS Biol* 4: 1201–1212, 2006.

London M, Hausser M. Dendritic computation. *Ann Rev Neurosci* 28: 503–532, 2005.

Magee JC, Carruth M. Dendritic voltage-gated ion channels regulate the action potential firing mode of hippocampal CA1 pyramidal neurons. *J Neurophysiol* 82: 1895–1901, 1999.

Mainen ZF, Sejnowski TJ. Influence of dendritic structure on firing pattern in model neocortical neurons. *Nature* 382: 363–366, 1996.

Manwani A, Koch C. Detecting and estimating signals in noisy cable structures. II. Information theoretical analysis. *Neural Comput* 11: 1831–1873, 1999.

Mehaffey WH, Doiron B, Maler L, Turner RW. Deterministic multiplicative gain control with active dendrites. *J Neurosci* 25: 9968–9977, 2005.

Metzner W, Koch C, Wessel R, Gabbiani F. Feature extraction by burst-like spike patterns in multiple sensory maps. *J Neurosci* 18: 2283–2300, 1998.

Nelson ME, MacIver MA. Prey capture in the weakly electric fish *Apteronotus albifrons*: sensory acquisiation strategies and electrosensory consequences. *J Exp Biol* 202: 1195–1203, 1999.

Noonan L, Doiron B, Laing C, Longtin A, Turner RW. A dynamic dendritic refractory period regulates burst discharge in the electrosensory lobe of weakly electric fish. *J Neurosci* 23: 1524–1534, 2003.

Oswald AMM, Chacron MJ, Doiron B, Bastian J, Maler L. Parallel processing of sensory input by bursts and isolated spikes. *J Neurosci* 24: 4351–4362, 2004.

Oswald AMM, Doiron B, Maler L. Interval coding. I. Burst Inter-spike intervals as idicators of stimulus intensity. *J Neurophysiol* 97: 2731–2743, 2007.

Perkel DH, Bullock TH. Neural coding. *Neurosci Res Prog Sum* 3: 405–527, 1968.

Pillow JW, Paninski L, Uzzell VJ, Simoncelli EP, Chichilnisky EJ. Prediction and decoding of retinal ganglion cell responses with a probabilistic spiking model. *J Neurosci* 25: 11003–11013, 2005.

Polsky A, Mel BW, Schiller J. Computational subunits in thin dendrites of pyramidal cells. *Nat Neurosci* 7: 621–627, 2004.

Poor HV. *An Introduction to Signal Detection and Estimation* (2nd ed.). New York: Springer, 1994.

Prescott SA, De Koninck Y. Gain control of firing rate by shunting inhibition: roles of synaptic noise and dendritic saturation. *Proc Natl Acad Sci USA* 100: 2076–2081, 2003.

Rashid AJ, Morales E, Turner RW, Dunn RJ. The contribution of dendritic Kv3 K^+ channels to burst threshold in a sensory neuron. *J Neurosci* 21: 125–135, 2001.

Reinagel P, Godwin D, Sherman M, Koch C. Encoding of visual information by LGN bursts. *J Neurophysiol* 81: 2558–2569, 1999.

Reyes AD. Influence of dendritic conductances on the input-output properties of neurons. *Annu Rev Neurosci* 24: 653–675, 2001.

Rieke F, Warland D, de Ruyter van Steveninck RR, Bialek W. Spikes: Exploring the Neural Code. Cambridge, MA: MIT Press, 1997.

Rinzel J, Ermentrout GB. Analysis of neural excitability and oscillations. In: *Methods in Neuronal Modeling* (2nd ed.), edited by Koch C, Segev I. Cambridge, MA: The MIT Press, 1998, p 251–291.

Sherman SM. Tonic and burst firing: dual modes of thalamocortical relay. *Trends Neurosci* 24: 122–126, 2001.

Stuart G, Spruston N, Sakmann B, Hausser M. Action potential initiation and backpropagation in neurons of the mammalian CNS. *Trends Neurosci* 20: 125–131, 1997.

Tan EW, Nizar JM, Carrera-G E, Fortune ES. Electrosensory interference in naturally occurring aggregates of a species of weakly electric fish, Eigenmannia virescens. *Behav Brain Res* 164: 83–92, 2005.

Tuckwell HC. Introduction to Theoretical Neurobiology I: Linear Cable Theory and Dendritic Structure. New York: Cambridge Univeristy Press, 1988.

Turner RW, Maler L, Deerinick T, Levinson SR, Ellisman MH. TTX-sensitive dendritic sodium channels underlie oscillatory discharge in a vertebrate sensory neuron. *J Neurosci* 14: 6453–6471, 1994.

Wang W, Jones HE, Andolina IM, Salt TE, Sillito AM. Functional alignment of feedback effects from visual cortex to thalamus. *Nat Neurosci* 9: 1330–1336, 2006.

Wessel R, Koch C, Gabbiani F. Coding of time-varying electric field amplitude modulations in a wave-type electric fish. *J Neurophysiol* 75: 2280–2293, 1996.